Journal of Materials Science & Technology 213 (2025) 146–152

Contents lists available at ScienceDirect

Journal of Materials Science & Technology

journal homepage: www.elsevier.com/locate/jmst

Research Article

Synchronously enhancing the plasticity and soft magnetism in Fe-based metallic glasses through memory effect

Weihua Zhou[a,1], Shiyuan Zhang[a,b,1], Lijian Song[c,d], Juntao Huo[c,d], Jun-Qiang Wang[c,d,*], Yi Li[a,*]

[a] Shenyang National Laboratory for Materials Science, Institute of Metal Research, Chinese Academy of Sciences, Shenyang 110016, China
[b] School of Materials Science and Engineering, University of Science and Technology of China, Shenyang 110016, China
[c] CAS Key Laboratory of Magnetic Materials and Devices, Zhejiang Province Key Laboratory of Magnetic Materials and Application Technology, Ningbo Institute of Materials Technology and Engineering, Chinese Academy of Sciences, Ningbo 315201, China
[d] Center of Materials Science and Optoelectronics Engineering, University of Chinese Academy of Sciences, Beijing 100049, China

ARTICLE INFO

Article history:
Received 23 February 2024
Revised 24 May 2024
Accepted 26 June 2024
Available online 6 July 2024

Keywords:
Memory effect
Rejuvenation
Reductilization
Soft magnetism
Fe-based metallic glass

ABSTRACT

Annealing has been a popular method to improve the soft magnetism of metallic glasses (MGs), which however usually makes MGs brittle and difficult to process. Here, it is demonstrated that the embrittled Fe-based MG can be reductilized and the coercivity can be further lowered through the rejuvenation of memory effect. The synchronous improvement in the plasticity and soft magnetic properties is attributed to the combination effects of releasing much residual stress, decreasing the magnetic anisotropy, and homogenizing the glasses during the rejuvenation process. The current work opens a new perspective to improve the properties of MGs by utilizing the memory effect and holds promising commercial application potential.

1. Introduction

Memory effect in amorphous materials is commonly observed and has been extensively studied [1–10]. The striking manifestation of the memory effect is its initial move away from equilibrium after two temperature steps of opposite sign, followed by the final approach to the equilibrium, first for volume observed by Kovas [11] and later for enthalpy by Hofer et al. [12]. This is to say that when a glass is annealed sequentially at two temperatures, i.e., first at a low temperature and then at a higher temperature, the glass can increase its volume or enthalpy initially during the second step of annealing [13]. During the process of memory effect, the properties of glasses can also be affected. The development of sub-T_g heat capacity peak in annealed glasses is also due to the memory effect. The reflective index of organic glass also shows a memory effect [2]. Despite this, property changes (e.g. mechanical or functional properties) during the process of memory effect are paid less attention.

This letter deals with an important yet overlooked aspect of the memory effect, i.e. its influence on the mechanical and magnetic properties of metallic glasses (MGs). The increase in the volume and enthalpy during the second step of annealing represents rejuvenation from its relaxed state to a high-energy state. We investigate the rejuvenation of the reductlization of embrittled Fe-based MGs. Our main result is that this rejuvenation lifts the energy state and restores the plasticity of the relaxed MG towards those of the as-cast MG, achieving reductilization of MG embrittled by annealing. Amazingly, the coercivity is further decreased after this rejuvenation. Our findings open a new perspective to tailor the properties of MGs by utilizing the memory effect and this provides an effective pathway to optimize the mechanical and soft magnetic properties of metallic glasses.

Soft magnetic Fe-based MGs, one typical example of metallic glasses, have attracted much attention in both scientific studies and practical applications due to their excellent soft magnetic properties, such as low coercivity (H_c), high saturation magnetic induction (B_s), low core loss (P), and excellent magnetic permeability (μ) [14–21]. However, the Fe-based MG ribbons have to be annealed at a temperature below the crystallization temperature (T_x) to release the internal stress and optimize their magnetic properties [15,16,22–25]. Unfortunately, such an annealing treatment usually leads to structural relaxation (annihilation of free volume), which in turn results in their embrittlement. The embrittled MGs are prone to fall off in the core lamination process and lead to in-

* Corresponding authors.
E-mail addresses: jqwang@nimte.ac.cn (J.-Q. Wang), liyi@imr.ac.cn (Y. Li).
[1] These authors contributed equally to this work.

https://doi.org/10.1016/j.jmst.2024.06.035
1005-0302/

complete magnetic circuits, short circuits, and other serious consequences [26–33]. Hence, resolving the embrittlement induced by structural relaxation is a key issue to the wide applications of soft magnetic Fe-based MG ribbons. We use this as an example material to demonstrate how the memory effect can be employed to reductilize the embrittled ribbons as well as to improve their soft magnetic properties.

2. Material and methods

2.1. Samples preparation

The Fe-based MG ribbons with a nominal composition of $Fe_{77.5}Si_{9.5}B_{13}$ (at.%) were provided by Advanced Technology & Materials Co. Annealing was carried out by thermal treatment of $Fe_{77.5}Si_{9.5}B_{13}$ MG ribbons at a temperature ranging from 580 K to 713 K (onset temperature of crystallization T_x = 800 K) for 1 h, which gives the relaxed samples. Two-step thermal treatment was carried out by first thermal treatment of Fe-based MG ribbons at 600 K for 1 h, and then heating them to a higher temperature ranging from 630 K to 780 K and quenching rapidly into ice-water, which gives the rejuvenated samples.

2.2. Thermal analysis

The thermal behaviors of as-quenched, relaxed, and rejuvenated specimens were investigated by differential scanning calorimetry (DSC, TA Q2000) at a heating rate of 20 K min^{-1}. Specimens were heated from room temperature up to 873 K to obtain the heat capacity (C_p) of the sample and then cooled to room temperature. A second run, under the same condition, was carried out to determine the baseline for each measurement. The enthalpy change (ΔH) relative to the as-quenched sample was calculated by subtracting the temperature integral of the heat flow curve of the relaxed or rejuvenated state from that of the as-quenched state [34,35].

$$\Delta H = -\int \left(C_{p,\ \text{treated}} - C_{p,\ \text{quenched}}\right) \mathrm{d}T \tag{1}$$

where $C_{p,\ \text{treated}}$ is the heat capacity of the respective relaxed or rejuvenated sample, $C_{p,\ \text{quenched}}$ is the heat capacity of the as-quenched sample, and the minus (–) means an energy reduction of relaxed and rejuvenated samples compared with that of the as-quenched sample.

2.3. Magnetic and mechanical testing

The magnetic induction and coercivity were measured using a B-H loop tracer (MATS 2010SD) under a maximum applied field of 800 A/m. Microhardness testing (Qness Q10 $A+$ microhardness tester, Vickers indenter) of the as-quenched, relaxed, and rejuvenated samples was conducted with a load of 10 g and a dwell time of 10 s. Bending tests for Fe-based MG ribbons were performed using a digital micrometer setup at room temperature similar to the work of Laws et al. [36]. The ribbons were clamped between two plates and then reduced the distance between plates. The ribbons would fail at different distances or not. The bending failure strain, ε_f, was evaluated as:

$$\varepsilon_f = t/\left(d_f - t\right) \tag{2}$$

where t is the thickness of the ribbon, and d_f is the fracture distance. For the case that ε= 1 % or 100 %, i.e. d_f= 2t, the ribbon is completely flexible. In order to ensure the accuracy of the data, each test was repeated more than 40 times. The surface morphologies of specimens after the bending test were characterized by scanning electron microscopy (Quanta 600 SEM, FEI) operated at an acceleration voltage of 20 kV.

2.4. Structural characterization

The structure of the as-quenched, relaxed, and rejuvenated samples was confirmed to be a fully amorphous structure by X-ray diffraction (XRD, Bruker D2 phaser) with Co-K_α radiation (wavelength: 0.1789 nm). TEM studies were carried out with a transmission electron microscopy (FEI Tecnai F20) operated at 200 kV. High-resolution transmission electron microscopy (HRTEM) image analysis was carried out using the software DigitalMicrograph3 of Gatan Inc. TEM specimens were thinned using ion milling at a temperature of –173 K.

2.5. Stress relaxation measurements

The isothermal stress relaxation tests of as-quenched, relaxed, and rejuvenated samples were performed on a dynamic mechanical analyzer (DMA, TA instrument Q800) in an argon-flushed atmosphere. During the stress relaxation, the isothermal temperature, step strain, and time span were set to be 650 K, 0.3 %, and 3600 s, respectively.

The stress relaxation process of glass can be described by Kohlrausch-Williams-Watts (KWW) function:

$$\frac{\sigma_{(t)}}{\sigma_{(0)}} = \exp\left(-\left(\frac{t}{\tau}\right)^{\beta_{\text{KWW}}}\right) \tag{3}$$

where $\sigma_{(t)}$ is the instantaneous stress at time t, $\sigma_{(0)}$ is the initial stress, τ is the characteristic relaxation time, and β_{KWW} is the non-exponential parameter, which reflects the dynamic heterogeneity of the glassy system.

Taking a twice logarithm on both sides of the above KWW equation as suggested by Gao et al. [37]:

$$\ln\left(\ln\left(\frac{\sigma_{(t)}}{\sigma_{(0)}}\right)\right) = \beta_{\text{KWW}} \ln(t) - \beta_{\text{KWW}} \ln(\tau) \tag{4}$$

The instantaneous values of β_{KWW} can be obtained by the derivative of $\ln(\ln(\sigma_{(t)}/\sigma_{(0)}))$ to $\ln(t)$.

3. Results and discussion

3.1. Annealing and rejuvenation processes

The key characteristic of the memory effect is its two steps of annealing, the first is to anneal it at a lower temperature, which results in relaxation; the subsequent second one is to anneal at a higher temperature to produce the memory effect, i.e. increase in volume and enthalpy [1,5]. Following the thermal protocol of the memory effect, we employed two steps of thermal annealing in the present work as illustrated by Fig. 1(a). The first-step thermal treatment is annealing an as-quenched $Fe_{77.5}Si_{9.5}B_{13}$ (at.%) ribbon at a low temperature (T_a) of 600 K for 1 h to attain a relaxed sample (This is usually necessary to optimize its magnetic properties). The second-step thermal treatment is thermal exposure of the relaxed sample at a higher temperature (rejuvenation temperature, T_{rej}) from 620 K to 780 K to rejuvenate the relaxed sample. The heat flow curves of the as-quenched, relaxed, and several typical rejuvenated samples during heating are displayed in Fig. 1(b), which mainly focuses on the temperature range of 425–820 K. It is found that the as-quenched sample possesses a significant exothermic peak, demonstrating the high energy state of the quenched ribbons. After the first-step thermal treatment, the exothermic peak disappears and is replaced by an endothermic peak, implying a reduction in the energy state of annealed ribbons. As expected, after the second-step thermal treatment, the endothermic peak weakens and disappears with increasing T_{rej}, indicating an increase in the energy state induced by the memory

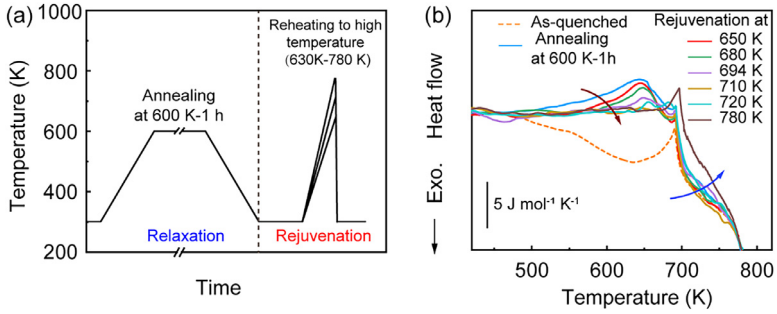

Fig. 1. (a) Scheme of the two-step thermal treatment process. The as-quenched MG ribbons were first annealed at 600 K for 1 h (relaxation), and the relaxed samples were then subsequently reheated to various high temperatures ranging from 630 to 780 K and quenched rapidly into iced water to obtain rejuvenated MGs. (b) Heat flow curves of the as-quenched, relaxed, and several typical rejuvenated samples in the temperature range of 425–820 K.

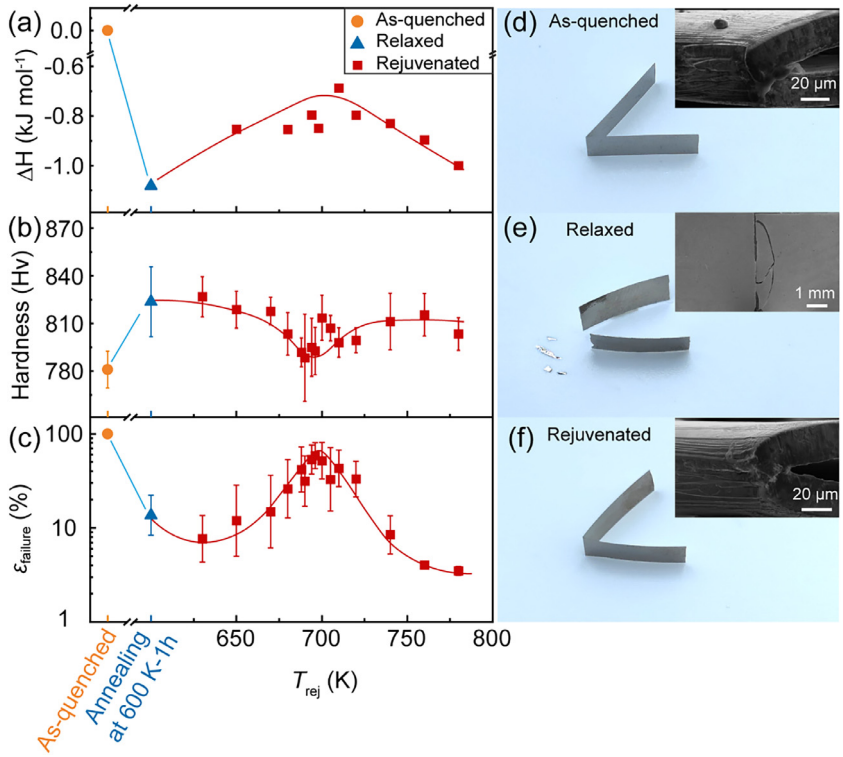

Fig. 2. (a) Enthalpy change relative to as-quenched sample (ΔH), (b) Vickers hardness, and (c) bending strain as a function of annealing and rejuvenation temperature. (d–f) Morphologies after bending tests of as-quenched, relaxed, and rejuvenated MG ribbons. The as-quenched ribbon is flexible and can be bent to 100 % without failure (d), after annealing, the ribbon shows brittle fracture by cracking into several pieces (e), however, after the rejuvenation at T_{rej}= 694 K, the brittle ribbon becomes flexible again (f). The insets in (d–f) show the close-up of the corner of the bent ribbons.

as reported by previous [5,10]. The fully amorphous structure of the as-quenched, relaxed, and rejuvenated samples was confirmed by X-ray diffraction patterns, high-resolution transmission electron microscopy (HRTEM) images, and corresponding selected area electron diffraction (SAED) patterns (Fig. S1 in Supplementary materials).

3.2. Non-monotonic variations of energy state and mechanical properties

Fig. 2(a) shows the variations of enthalpy change (ΔH), which is obtained from the area of heat flow curves between the annealed sample and the as-quenched sample as illustrated by Fig. S2. After *first* annealing at 600 K for 1 h, the ΔH was decreased to –1.08 kJ mol^{-1}, confirming a reduction in the energy state induced by the annealing and implying structure relaxation. However, after the subsequent thermal exposure of the relaxed sample at a higher temperature (T_{rej}), the ΔH did not continue to decrease but increased, the same as for the known memory effect, confirming that this *second* annealing lifts the energy state of the relaxed sample towards that of the as-quenched sample. The increase in energy state demonstrates that rejuvenation instead of relaxation has occurred during the second annealing of the relaxed sample at a higher temperature. Furthermore, as the T_{rej} increases, the ΔH peaks at –0.8 kJ mol^{-1} at the T_{rej} of around 700 K, implying an optimal rejuvenation effect at this T_{rej}. It is noted that the ΔH is still negative, indicating that the energy states of rejuvenated samples remain lower than that of the as-quenched sample.

It is well accepted that relaxation hardens and embrittles MGs, while rejuvenation softens and toughens them [38–41]. To investigate the effect of first annealing and subsequent rejuvenation on the mechanical properties of Fe-based MG ribbons, hardness measurements were carried out and the corresponding results are shown in Fig. 2(b). After first annealing at T_a= 600 K for 1 h, the hardness increased by 5.6 %, from 780.0 ± 11.6 HV for the as-quenched sample to 823.7 ± 22.0 HV for the relaxed sample.

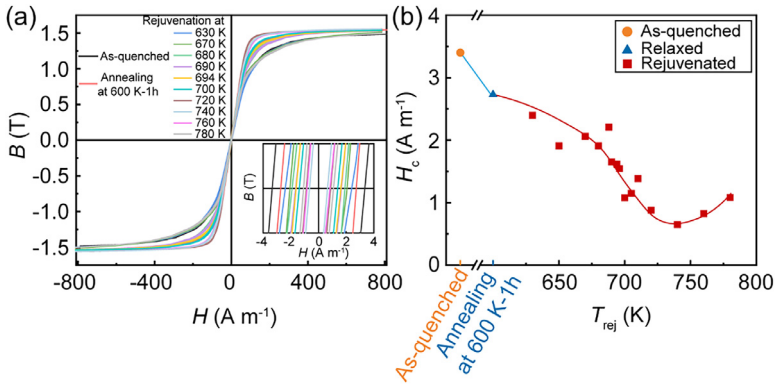

Fig. 3. (a) Magnetic hysteresis loops for the as-quenched, relaxed, and rejuvenated MG ribbons. (b) Coercivity as a function of annealing and rejuvenation temperature.

Upon rejuvenation of the relaxed sample, the hardness of rejuvenated samples generally decreases towards that of the as-quenched sample. As shown in Fig. 2(b), there is a minimum hardness of 788.4 ± 27.5 HV after rejuvenation at around 700 K, which is close to but still higher than that of the as-quenched sample. The hardness minimum matches the maximum in the ΔH shown in Fig. 2(a).

Furthermore, we systemically investigated the effect of first annealing and rejuvenation on the bending strain of the Fe-based MG ribbons. The bending strain was determined by a two-point bending test (see 2.3 section). Fig. 2(c) shows the variation of bending strain for the as-quenched, relaxed, and rejuvenated samples. All the as-quenched samples are completely flexible and can be bent to a bending strain of 100 % without failure. After first annealing, the bending strain of the relaxed MG ribbons is reduced to an average value of 15 % ± 6 %, confirming their embrittlement induced by structural relaxation. However, after the subsequent rejuvenation, the bending strain of the rejuvenated samples is revived. The maximum average bending strain of 65 % ± 26 %, which is four times that of 15 % ± 6 % of the relaxed sample, is obtained for the sample rejuvenated at T_{rej} of around 700 K. The variation trend of bending strain well coincides with the variation trend of energy state as well as that of hardness, that the higher the energy state is and the lower the hardness is, the better the plasticity is.

Fig. 2(d–f) shows the fracture morphologies of as-quenched, relaxed, and rejuvenated samples, respectively. For the as-quenched sample, the ribbon is completely flexible (Fig. 2(d)). The surface around the tip exhibits abundant shear bands (inset in Fig. 2(d)). After annealing, the ribbon cracks into several pieces (Fig. 2(e)), coinciding with its low bending strain and demonstrating its brittleness. However, after the rejuvenation of the relaxed ribbons, ribbons became flexible again (Fig. 2(f)), and abundant shear bands reappeared on the tip of the bent ribbon (inset in Fig. 2(f)), confirming that the rejuvenation can induce reductilization of the relaxed MG. The whole process of embrittlement and reductilization can be seen in Video S1. These are consistent with the results of the bending strain observed in Fig. 2(c).

3.3. Continuous improvement in the soft magnetic properties

As reported previously the annealing would significantly affect the magnetic properties of the Fe-based soft magnetic ribbons [15,25–27,30,32,42–45], we have also systematically investigated the effect of the present two consecutive annealing on magnetic properties of the as-quenched, relaxed and rejuvenated Fe-based MG ribbons by measuring their magnetic hysteresis loops and the corresponding results are shown in Fig. 3(a). It is shown that first annealing can slightly improve the saturation magnetic induction (B_s) from 1.48 T of the as-quenched sample to 1.54 T of the relaxed sample, while the subsequent rejuvenation has no significant influence on the B_s, which remains to be 1.54 T. The variation trend of coercivity measured on the magnetic hysteresis loops with annealing and rejuvenation temperatures is shown in Fig. 3(b). The as-quenched sample possesses a maximum value of 3.4 A m^{-1}. After first annealing at 600 K for 1 h, the coercivity of the relaxed sample decreases to 2.7 A m^{-1}, confirming the usual effect of relaxation on improving the soft magnetic properties of Fe-based MGs [22,23,28]. Upon second annealing i.e. rejuvenation of the relaxed MG at different T_{rej}, the coercivity keeps on decreasing with the increasing T_{rej} and shows a minimum of 0.8 A m^{-1} at a T_{rej} of around 740 K, however, with a further increase in T_{rej}, the coercivity increases but is still much lower than that of 2.7 A m^{-1} for the relaxed sample. This implies that rejuvenation did not deteriorate but continued to improve the soft magnetic properties, significantly. The continuous decrease in the coercivity in the rejuvenated samples in the present work is unexpected because rejuvenation by other methods usually has little and even negative influence on reducing coercivity [26,46,47].

3.4. Breaking the trade-off between magnetic properties and plasticity in relaxed MGs

Improving the soft magnetic properties of Fe-based MG ribbons by annealing has been widely reported in previous works [15,22,23,25,28,44,45,48,49]. However, this was achieved at the expense of their plasticity. Fig. 4 summarizes the variation of bending strain along with coercivity during the annealing of different kinds of Fe-based MG ribbons reported previously [15,26,30,32,42,44]. For each MG, the bending strain decreases with decreasing coercivity, displaying a typical trade-off as illustrated by the dashed gray and brown lines. Our study of the annealing temperature dependence of coercivity and bending strain in $Fe_{77.5}Si_{9.5}B_{13}$ MG ribbons confirmed this trade-off too. It is shown that, at the constant annealing time of 1 h, the coercivity shows a decreasing trend with increasing annealing temperature, while, the bending strain is completely lost once the annealing temperature is higher than 610 K (Fig. S3). Rejuvenation, the opposite process of aging, provides an opportunity to resolve the embrittlement induced by structural relaxation. Although several rejuvenation methods, such as irradiation [50–53], room temperature rolling [54] and cryogenic thermal cycling [26,46,55,56] have been successfully applied to toughen the Fe-based MGs, they have little and even negative influence on decreasing coercivity [26,46]. The trade-off between bending strain and coercivity remains. Our present work shows that rejuvenation through the memory effect by a further thermal exposure of the relaxed MG at a temperature higher than T_a not only rejuvenated the relaxed ribbons and thus restored their bending strain, but also intriguingly further lowered the coercivity as

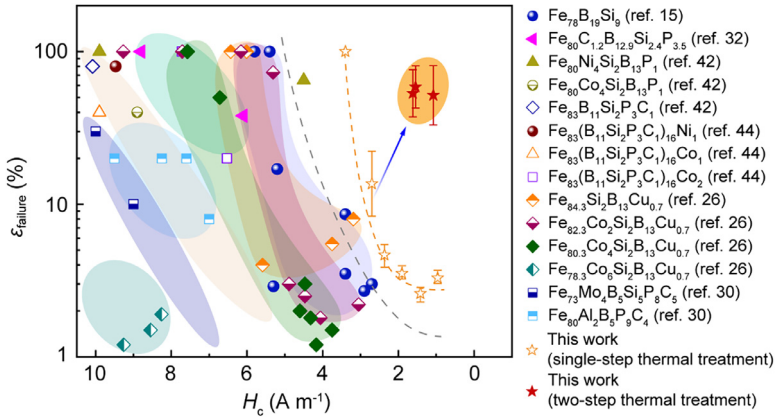

Fig. 4. Comparison of bending strain versus coercivity of the current Fe-based metallic glass ribbons after single-step thermal treatment and two-step thermal treatment with other Fe-based metallic glass ribbons after single-step thermal treatment. For single-step thermal treatment, the bending strain decreases with decreasing coercivity for various Fe-based metallic glass ribbons, [15,26,30,32,42,44] showing the trade-off between bending strain and coercivity as illustrated by gray and brown dashed line. Our present work shows that the two-step thermal treatment (Red solid stars) can break this trade-off, achieving a decrease in coercivity and improvement in the ductility of the relaxed ribbons.

indicated by the blue arrow, so to break the traditional trade-off between plasticity and coercivity.

3.5. Evolusion of stress relief and magnetic anisotropy during two steps of thermal treatment

It has been reported widely that significant internal stress exists in the Fe-based ribbons in the as-rapidly-quenched state. It has a detrimental influence on their soft magnetic properties by resisting the arrangement of magnetic domains when applied magnetic field [22,23,28,48,57]. Here, the stress relief during annealing and rejuvenation processes is investigated according to the method in reference [22]. Fig. 5(a) shows that annealing at 600 K for 1 h can significantly release the quenched-in internal stress by 74.9 % ± 0.3 %. Upon the subsequent rejuvenation, the internal stress was further released. The extra fraction of stress relief shows a significant temperature dependence. With the increase in T_{rej}, the fraction of stress relief increases sharply at temperatures higher than 700 K.

According to Suzuki et al. [58], the magnetic anisotropy, K_u, is closely related to the H_c of amorphous materials. A lower K_u usually yields a lower H_c. Fig. 5(b) shows the magnetic anisotropy estimated through the energy required to attain the magnetic saturation as illustrated in the inset Figure [59–62]. The as-quenched sample has the largest value of 154 J m^{-3}. After annealing at 600 K for 1 h, the value of K_u decreases to 115 J m^{-3}. Amazingly but also as expected, the K_u decreases sharply when the sample is rejuvenated around 700 K, with a minimum value of about 90 J m^{-3} for the sample rejuvenated at T_{rej}= 720 K. This trend matches the evolution of coercivity in Fig. 3(b). Thus, releasing the internal stress can decrease the magnetic anisotropy and then decrease the coercivity.

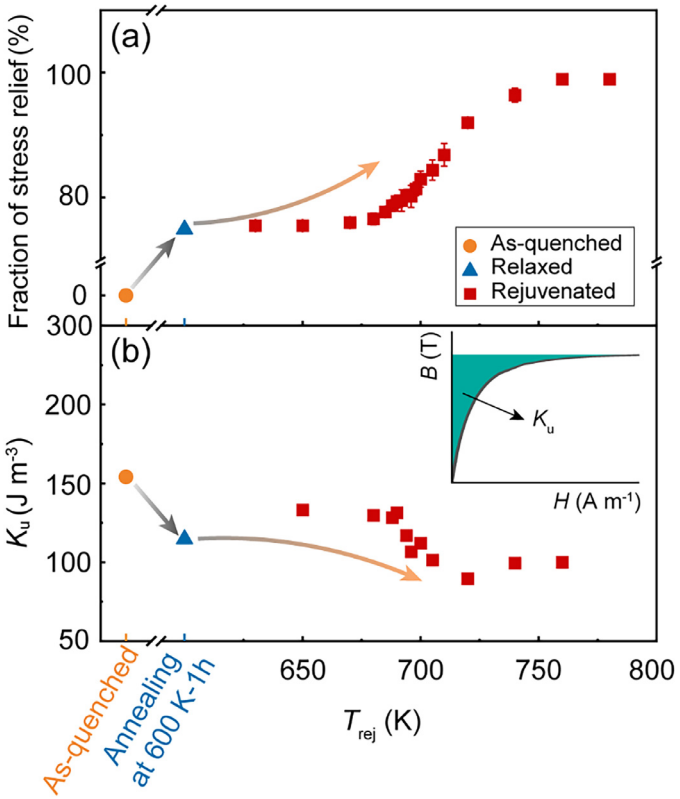

Fig. 5. (a) The fraction of stress relief and (b) magnetic anisotropy as a function of annealing and rejuvenation temperature. The inset illustrates the measurement of magnetic anisotropy K_u in the B–H curve.

3.6. Evolution of homogeneity during two steps of thermal treatment

It has been well-known there are nanoscale fluctuations in glasses [63], which hinder the motion of domain walls [24,64]. Here we use the instantaneous heterogeneity parameter β_{KWW} in the Kohlrausch-Williams-Watts (KWW) equation to study the heterogeneity of metallic glass after rejuvenation, as shown in Fig. 6(a). The instantaneous β_{KWW} for the as-cast, annealed, and rejuvenated metallic glasses are calculated based on the stress relaxation curve according to Gao et al. [37]. The as-cast sample has an instantaneous β_{KWW} of about 0.62, denoting a heterogeneous characteristic. After annealing at 600 K for 1 h, the instantaneous β_{KWW} for the relaxed metallic glasses increases to about 0.8, suggesting the increase in homogeneity. After the rejuvenation at a higher temperature of 720 K, the instantaneous β_{KWW} for the rejuvenated metallic glasses increases to about 0.98, suggesting a further increase in homogeneity. The increase in homogeneity should be responsible for the enhanced soft magnetism, e.g. decrease in coercivity. The evolution of homogeneity of metallic glasses is illustrated in Fig. 6(b) in the enthalpy phase diagram. During isothermal annealing, the enthalpy ages down first in β relaxation kinetics and then experiences the α relaxation stage [5,65]. Recently,

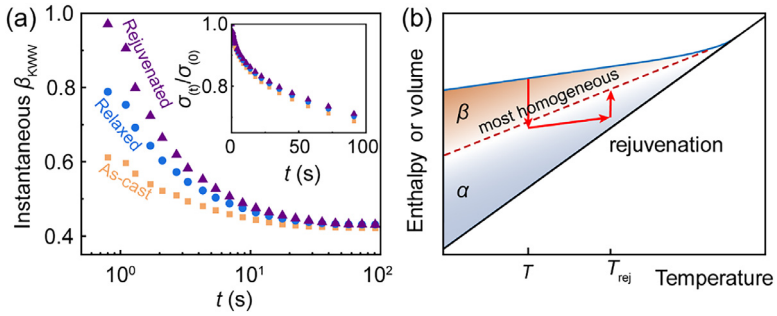

Fig. 6. (a) The instantaneous homogeneity parameter β_{KWW} for the as-cast, relaxed, and rejuvenated amorphous alloys along with annealing time. The rejuvenated sample is the most homogeneous with an initial β_{KWW} of about 0.98. Inset is the stress relaxation curve for the three samples. (b) Schematic illustration for the enthalpy rejuvenation during a two-step annealing. In the transition region (marked by the dashed line) between β relaxation (yellow shaded zone) and α relaxation region (blue shaded zone), the glass is the most homogeneous according to reference [66].

Tong, et al. [66] found that glasses become the most homogeneous during annealing till the end of β relaxation stage. When rejuvenation at a higher temperature, the α relaxation will be reactivated towards a more homogeneous state with a larger β_{KWW} value [66]. Thus, after rejuvenation, the more homogeneous state allows the domain walls easier to move that yields a superior soft magnetic property; the rejuvenated high energy state produces more free volume that yields good plasticity.

4. Conclusions

In summary, a combination of increasing plasticity and enhancing soft magnetism has been realized through the rejuvenation of memory effect, which has broken the long-lasting trade-off relationship between plasticity and soft magnetism in Fe-based metallic glasses. The two-step annealing strategy is simple yet surprisingly effective to restore the plasticity and, synchronously, to improve the soft magnetic properties and hold a promising future for commercial applications. The co-improvement in plasticity and soft magnetism after rejuvenation is attributed to the combination effects of releasing much residual stress, decreasing the magnetic anisotropy, and homogenizing the glasses. Besides, as the memory effect has been widely observed in amorphous materials including metallic glasses, polymeric, and ceramic materials, it is conceivable that the present rejuvenation method could be employed to optimize the mechanical as well as functional properties in other amorphous materials.

Declaration of competing interest

The authors declare that they have no known competing financial interests or personal relationships that could have appeared to influence the work reported in this paper.

CRediT authorship contribution statement

Weihua Zhou: Conceptualization, Data curation, Formal analysis, Investigation, Methodology, Writing – original draft, Writing – review & editing. **Shiyuan Zhang:** Conceptualization, Data curation, Formal analysis, Investigation, Methodology, Writing – original draft, Writing – review & editing. **Lijian Song:** Conceptualization, Data curation, Formal analysis, Methodology. **Juntao Huo:** Conceptualization, Methodology, Project administration, Visualization. **Jun-Qiang Wang:** Funding acquisition, Project administration, Visualization, Writing – original draft, Writing – review & editing, Conceptualization. **Yi Li:** Conceptualization, Funding acquisition, Project administration, Visualization, Writing – original draft, Writing – review & editing.

Data availability

The data that support the findings of this study are available from the corresponding author upon reasonable request.

Acknowledgements

The authors acknowledge financial support from the Shenyang National Laboratory for Materials Science. Yi Li and Junqiang Wang acknowledge financial support from the National Natural Science Foundation of China (No. 52231006). Junqiang Wang acknowledges financial support from the National Key R&D Program of China (No. 2018YFA0703600), and the National Natural Science Foundation of China (Nos. 92163108 and 52222105). We thank Yonghua Meng (SYNL, IMR, China) for the making of the movie.

Supplementary materials

Supplementary material associated with this article can be found, in the online version, at doi:10.1016/j.jmst.2024.06.035.

References

[1] A.J. Kovacs, J.J. Aklonis, J.M. Hutchinson, A.R. Ramos, J. Polym. Sci., Polym. Phys. Ed. 17 (1979) 1097–1162.
[2] L. Boesch, A. Napolita, P.B. Macedo, J. Am. Ceram. Soc. 53 (1970) 148–&.
[3] C.T. Moynihan, P.B. Macedo, C.J. Montrose, C.J. Montrose, P.K. Gupta, M.A. DeBolt, J.F. Dill, B.E. Dom, P.W. Drake, A.J. Easteal, P.B. Elterman, R.P. Moeller, H. Sasabe, J.A. Wilder, Ann. N.Y. Acad. Sci. 279 (1976) 15–35.
[4] A.L. Greer, J.A. Leake, J. Non-Cryst. Solids 33 (1979) 291–297.
[5] L. Song, W. Xu, J. Huo, F. Li, L.M. Wang, M.D. Ediger, J.Q. Wang, Phys. Rev. Lett. 125 (2020) 135501.
[6] Y.V. Pershin, M. Di Ventra, Adv. Phys. 60 (2011) 145–227.
[7] M. Adhikari, S. Sastry, Eur. Phy. J. E 41 (2018) 105.
[8] P. Luo, Y.Z. Li, H.Y. Bai, P. Wen, W.H. Wang, Phys. Rev. Lett. 116 (2016) 175901.
[9] L. Wang, Z. Wang, L. Hu, Intermetallics 156 (2023) 107864.
[10] Y.H. Meng, S.Y. Zhang, W.H. Zhou, J.H. Yao, S.N. Liu, S. Lan, Y. Li, Acta Mater. 241 (2022) 118376.
[11] A.J. Kovacs, J. Polym. Sci. 30 (1958) 131–147.
[12] K. Hofer, J. Perez, G.P. Johari, Philos. Mag. Lett. 64 (1991) 37–43.
[13] I.M. Hodge, J. Non-Cryst. Solids 169 (1994) 211–266.
[14] H.X. Li, Z.C. Lu, S.L. Wang, Y. Wu, Z.P. Lu, Prog. Mater. Sci. 103 (2019) 235–318.
[15] X. Tong, Y. Zhang, Y. Wang, X. Liang, K. Zhang, F. Zhang, Y. Cai, H. Ke, G. Wang, J. Shen, A. Makino, W. Wang, J. Mater. Sci. Technol. 96 (2022) 233–240.
[16] L. Zhu, S.S. Jiang, Z.Z. Yang, G.B. Han, S.S. Yan, Y.G. Wang, J. Magn. Magn. Mater. 519 (2021) 167513.
[17] K. Suzuki, A. Makino, A. Inoue, T. Masumoto, J. Appl. Phys. 70 (1991) 6232–6237.
[18] J.M. Silveyra, E. Ferrara, D.L. Huber, T.C. Monson, Science 362 (2018) eaao0195.
[19] X. Li, G. Shan, C.H. Shek, J. Mater. Sci. Technol. 103 (2022) 113–120.
[20] X. Jia, B. Zhang, W. Zhang, Y. Dong, J. Li, A. He, R.-W. Li, J. Mater. Sci. Technol. 108 (2022) 186–195.
[21] X. Fan, T. Zhang, W. Yang, J. Luan, Z. Jiao, H. Li, J. Mater. Sci. Technol. 147 (2023) 124–131.
[22] M.C. Ri, D.W. Ding, S. Sohrabi, B.A. Sun, W.H. Wang, J. Appl. Phys. 124 (2018) 165108.
[23] M.C. Ri, D.W. Ding, B.A. Sun, J.Q. Wang, X.S. Zhu, B.B. Wang, T.L. Wang, Q.Q. Qiu, L.S. Huo, W.H. Wang, J. Non-Cryst. Solids 495 (2018) 54–58.

[24] N. He, L. Song, W. Xu, J. Huo, J.-Q. Wang, R.-W. Li, J. Non-Cryst. Solids 509 (2019) 95–98.
[25] Q. Luo, D. Li, M. Cai, S. Di, Z. Zhang, Q. Zeng, Q. Wang, B. Shen, J. Mater. Sci. Technol. 116 (2022) 72–82.
[26] H. Zheng, L. Zhu, S.S. Jiang, Y.G. Wang, F.G. Chen, J. Alloys Compd. 790 (2019) 529–535.
[27] C. Minnert, M. Kuhnt, S. Bruns, A. Marshal, K.G. Pradeep, M. Marsilius, E. Bruder, K. Durst, Mater. Des. 156 (2018) 252–261.
[28] C. Wang, Z. Wu, X. Feng, Z. Li, Y. Gu, Y. Zhang, X. Tan, H. Xu, Intermetallics 118 (2020) 106689.
[29] R. Gerling, F.P. Schimansky, R. Wagner, Acta Metall. 36 (1988) 575–583.
[30] C.Y. Liu, Y.X. Zhang, C.Y. Zhang, J. Kang, G. Yuan, R.D.K. Misra, Intermetallics 132 (2021) 107144.
[31] F.E. Luborsky, H.H. Liebermann, Mater. Sci. Eng. 49 (1981) 257–261.
[32] X. Liang, A. He, A. Wang, J. Pang, C. Wang, C. Chang, K. Qiu, X. Wang, C.-T. Liu, J. Alloys Compd. 694 (2017) 1260–1264.
[33] J. Zhou, S. Di, B. Sun, Q. Zeng, B. Shen, J. Mater. Sci. Technol. 65 (2021) 54–60.
[34] M.X. Li, P. Luo, Y.T. Sun, P. Wen, H.Y. Bai, Y.H. Liu, W.H. Wang, Phys. Rew. B 96 (2017) 174204.
[35] Z. Evenson, R. Busch, Acta Mater. 59 (2011) 4404–4415.
[36] K.J. Laws, D. Granata, J.F. Löffler, Acta Mater. 103 (2016) 735–745.
[37] Y.R. Gao, Y. Tong, L.J. Song, X.X. Shui, M. Gao, J.T. Huo, J.Q. Wang, Scr. Mater. 224 (2023) 115114.
[38] S.V. Ketov, Y.H. Sun, S. Nachum, Z. Lu, A. Checchi, A.R. Beraldin, H.Y. Bai, W.H. Wang, D.V. Louzguine-Luzgin, M.A. Carpenter, A.L. Greer, Nature 524 (2015) 200–203.
[39] J. Pan, Y.X. Wang, Q. Guo, D. Zhang, A.L. Greer, Y. Li, Nat. Commun. 9 (2018) 560.
[40] G. Kumar, D. Rector, R.D. Conner, J. Schroers, Acta Mater. 57 (2009) 3572–3583.
[41] P. Murali, U. Ramamurty, Acta Mater. 53 (2005) 1467–1478.
[42] H. Zheng, L. Zhu, S.S. Jiang, Y.G. Wang, S.N. Liu, S. Lan, F.G. Chen, J. Alloys Compd. 816 (2020) 152549.
[43] T. Wang, L. Zhang, Q. Hou, Q. Hao, J. Qiao, J. Non-Cryst. Solids 569 (2021) 120965.
[44] P. Chen, T. Liu, F. Kong, A. Wang, C. Yu, G. Wang, C. Chang, X. Wang, J. Mater. Sci. Technol. 34 (2018) 793–798.
[45] J. Ge, Y. Gu, Z. Yao, S. Liu, H. Ying, C. Lu, Z. Wu, Y. Ren, J.-i. Suzuki, Z. Xie, Y. Ke, J. Zeng, H. Zhu, S. Tang, X.-L. Wang, S. Lan, J. Mater. Sci. Technol. 176 (2024) 224–235.
[46] S. Di, Q. Wang, Y. Yang, T. Liang, J. Zhou, L. Su, K. Yin, Q. Zeng, L. Sun, B. Shen, J. Mater. Sci. Technol. 97 (2022) 20–28.
[47] M.C. Ri, D.W. Ding, Y.H. Sun, W.H. Wang, J. Mater. Sci. Technol. 69 (2021) 1–6.
[48] D. Azuma, R. Hasegawa, S. Saito, M. Takahashi, J. Appl. Phys. 113 (2013) 17a339.
[49] F. Luborsky, J. Becker, R. McCary, IEEE Trans. Magn. 11 (1975) 1644–1649.
[50] R. Gerling, F.P. Schimansky, R. Wagner, Acta Metall. 35 (1987) 1001–1006.
[51] I. Skorvanek, R. Gerling, IEEE Trans. Magn. 30 (1994) 548–551.
[52] H. Zhang, X. Mei, X. Zhang, X. Li, Y. Wang, J. Sun, Y. Wang, Nucl. Instrum. Meth. B 375 (2016) 79–86.
[53] X. Zhang, T. Guan, L. Zhang, X. Mei, Y. Wang, Surf. Coat. Technol. 389 (2020) 125609.
[54] Y. Guo, D. Ma, X. Li, L. Lu, Y. Gao, Y. Shen, T. Zhang, J. Non-Cryst. Solids 596 (2022) 121875.
[55] S. Di, Q. Wang, J. Zhou, Y. Shen, J. Li, M. Zhu, K. Yin, Q. Zeng, L. Sun, B. Shen, Scr. Mater. 187 (2020) 13–18.
[56] S. Di, H. Ke, Q. Wang, J. Zhou, Y. Zhao, B. Shen, Mater. Des. 222 (2022) 111074.
[57] D.R. Huang, J.C.M. Li, Scr. Metall. 24 (1990) 1137–1142.
[58] K. Suzuki, J.M. Cadogan, Phys. Rew. B 58 (1998) 2730–2739.
[59] C.D. Graham Jr., T. Egami, R.S. Williams, Y. Takei, AIP Conf. Proc. 29 (1976) 218–219.
[60] R. Williams, T. Egami, IEEE Trans. Magn. 12 (1976) 927–929.
[61] Z. Xue, X. Li, S. Sohrabi, Y. Ren, W. Wang, Metals 10 (2020) 122.
[62] J. Xu, S. Kang, J. Wang, F. Xu, C. Shi, K. Zhang, J. Wang, Z. Chen, J. He, Z. Sun, J. Magn. Magn. Mater. 576 (2023) 170762.
[63] F. Zhu, H.K. Nguyen, S.X. Song, D.P.B. Aji, A. Hirata, H. Wang, K. Nakajima, M.W. Chen, Nat. Commun. 7 (2016) 11516.
[64] S. Ouyang, L.J. Song, Y.H. Liu, J.T. Huo, J.Q. Wang, W. Xu, J.L. Li, C.T. Wang, X.M. Wang, R.W. Li, Phys. Rev. Mater. 2 (2018) 063601.
[65] L.J. Song, Y. Gao, P. Zou, W. Xu, M. Gao, Y. Zhang, J.T. Huo, F.S. Li, J.C. Qiao, L.-M. Wang, J.-Q. Wang, Proc. Natl. Acad. Sci. U. S. A. 120 (2023) e2302776120.
[66] Y. Tong, F. Li, L. Song, Y. Liu, J. Huo, J. Qiao, Y. Yao, J.M. Pelletier, D. Crespo, E. Pineda, J.-Q. Wang, J. Mater. Sci. Technol. 177 (2023) 96–102.